Available online at www.sciencedirect.com
SCIENCE DIRECT®
ELSEVIER
International Journal of Impact Engineering 31 (2005) 1152–1171
INTERNATIONAL JOURNAL OF IMPACT ENGINEERING
www.elsevier.com/locate/ijimpeng

The use of metal foam projectiles to simulate shock loading on a structure

D.D. Radford, V.S. Deshpande, N.A. Fleck*

Department of Engineering, University of Cambridge, Trumpington St., Cambridge CB2 1PZ, UK

Received 14 November 2003; received in revised form 20 July 2004; accepted 22 July 2004
Available online 7 October 2004

Abstract

Metal foam projectiles are used to generate dynamic pressure–time histories representative of shock loading in water and air. A 1D plastic shock wave analysis is performed for a foam projectile impacting a free but rigid mass. It is shown that the pressure versus time pulse exerted on the mass and the shock arrest distance within the foam depend upon the ratio of foam mass to impacted mass, and upon the ratio of quasi-static to hydrodynamic strength of the foam. The theory is supported by two sets of experiments, one where Alporas foam impacts an instrumented Kolsky pressure bar, and one where the foam is fired at a free mass. It is demonstrated that the magnitude and duration of the pressure pulse can be controlled by suitable adjustment of the velocity, length and density of the foam projectile.

Keywords: Metal foams; Shock; Structures; Dynamic loading

1. Introduction

There is continued interest in the development of shock resistant structures, in order to maximise survivability both of the structure and of any occupants. In order to validate models and to test prototypes at the laboratory scale, there has been a long-standing need to develop a simple, economical and safe experimental technique to dynamically load a structure with pressure

*Corresponding author. Tel.: +44-1223-332650; fax: +44-1223-332662.
E-mail address: naf1@eng.cam.ac.uk (N.A. Fleck).

0734-743X/$ - see front matter © 2004 Elsevier Ltd. All rights reserved.
doi:10.1016/j.ijimpeng.2004.07.012

histories, which are representative of air and water shock. Typically in the shock loading of a fluid upon a structure, the primary pressure pulse is exponentially decaying in shape with a peak value of 10–300 MPa, and a decay time on the order of 0.1 ms, as discussed by Ashby et al. [1] and Fleck and Deshpande [2].

Recent research by Ashby et al. [1] and by Tan et al. [3] has revealed that metal foams collapse at almost constant pressures; the magnitude of this pressure increases from a few MPa at quasi-static loading rates to a pressure on the order of hundreds of MPa when the loading speed is increased to a few hundred metres per second due to the propagation of a shock wave. The density of the foam provides an additional parameter for controlling the collapse pressure.

There is a substantial literature on shock wave propagation in cellular systems. Following the work on structural shocks in ring systems by Reid et al. [4,5], Reid et al. [6] analysed shock wave propagation in cellular solids such as assemblies of metal tubes and honeycombs while Zaretsky and Ben-Dor [7] analysed shock wave propagation in polymer foams. More recently, Ashby et al. [1] and by Tan et al. [3] applied such an analysis to investigate shock wave propagation in metal foams assuming a ''rigid–perfectly plastic locking'' solid; this was subsequently extended to an ''elastic–perfectly plastic-locking'' analysis by Lopatnikov et al. [8,9].

The current study explores the potential of using metal foams to dynamically load a structure. Circular, cylindrical aluminium foam projectiles are easy to manufacture and are relatively economical. First, a one-dimensional plastic shock wave analysis is performed for the impact of a metal foam cylinder on a free but rigid mass. For the limiting case of an infinite target mass, this represents the impact of a Kolsky pressure bar. The analysis predicts the pressure versus time history on the mass, and the plastic shock arrest distance within the foam projectile. Second, the predicted behaviour is compared to the measured behaviour of Alporas aluminium foam projectiles impacting a Kolsky bar and impacting a free mass. The pressure history is measured using the Kolsky bar as a dynamic load cell, while the displacement of the impacted mass is observed by high-speed photography.

2. Plastic shock wave model for the impact of a foam

Consider a foam projectile of length L, unit cross-section and mass m, impinging a rigid unsupported mass M also of unit cross-section, as sketched in Fig. 1a. Initially, the mass is stationary while the projectile has an approach velocity v_0. It is assumed that the foam has a quasi-static compressive stress versus strain characteristic under uniaxial straining as sketched in Fig. 1b: the foam has an infinite elastic modulus, a constant plateau stress σ_Y and a nominal densification strain ε_D. After this strain has been attained the foam locks up, and the tangent modulus is again infinite. Typically, metallic foams have a plastic Poisson ratio, which is close to zero, and so the uniaxial response for uniaxial straining (with zero transverse strain) is close to that for uniaxial compressive stressing (with zero transverse stress).

We seek an expression for the contact pressure between the foam and free mass as a function of time. It is assumed that a plastic shock wave enters the foam from the impact face and travels along the axis of the foam projectile at a speed $c(t)$ with increasing time t. Introduce the term *incident* for the portion of the foam moving with the mass and downstream of the shock wave, travelling at a velocity $v_i(t)$, as shown in Fig. 1a. Similarly, the *distal* portion of the foam is

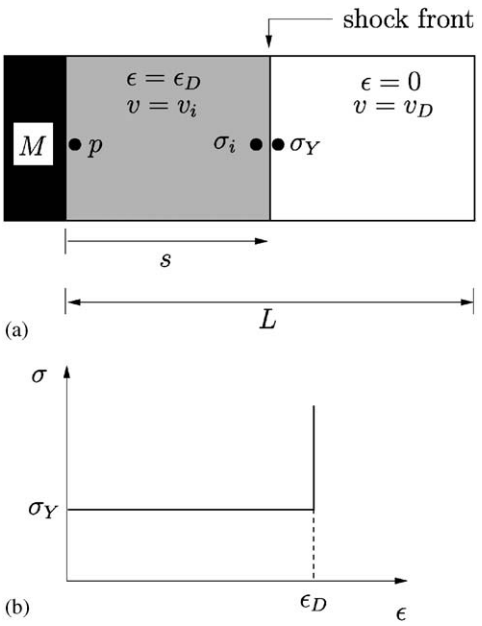

Fig. 1. (a) Sketch of the propagation of a one-dimensional shock wave in a foam impacting a free mass. (b) Idealised quasi-static stress versus strain response of the metal foam.

upstream of the shock wave and travels with a velocity $v_D(t) > v_i(t)$. At any instant, the foam is non-deforming except for a jump in compressive strain of magnitude ε_D across the shock wave. Associated with the jump in strain is a jump in stress: σ_i is the stress on the downstream face of the shock wave and we assume that the foam is at yield on the upstream face of the shock due to the propagation of elastic waves, as discussed in Ashby et al. [1] and by Tan et al. [3]. After a time t, the shock wave has travelled a distance s along the foam, as measured in the undeformed configuration. We proceed to analyse the shock wave propagation in the foam employing a Lagrangian framework (i.e. write equilibrium using the undeformed configuration as the reference).

In the one-dimensional problem under consideration, where the plastic Poisson's ratio of the foam is assumed to be zero, the Cauchy and nominal stresses are identical and the equation of motion is written as

$$\frac{\partial \sigma}{\partial X} = -\rho \frac{\partial^2 u}{\partial t^2}, \tag{1a}$$

where X is the position of material point in the undeformed configuration, u is displacement, ρ the original density of the foam, and σ the nominal (or Cauchy) stress. Integrating Eq. (1a) over the range $L - s \leqslant X \leqslant L$ and noting that the foam is rigid over this range, gives the relation between the acceleration of the distal end $\dot{v}_D$ and the quasi-static yield strength σ_Y as

$$m\left(1 - \frac{s}{L}\right)\dot{v}_D = -\sigma_Y \tag{1b}$$

or, in non-dimensional form,

$$(1-\bar{s})\frac{\mathrm{d}\bar{v}_{\mathrm{D}}}{\mathrm{d}\bar{s}} = -\frac{\sigma_{\mathrm{Y}}}{\rho c v_0}, \tag{1c}$$

where $\bar{s} \equiv s/L$ and $\bar{v}_{\mathrm{D}} \equiv v_{\mathrm{D}}/v_0$. In order to integrate Eq. (1b) it is necessary to obtain an expression for c in terms of $\bar{v}_{\mathrm{D}}$. Mass conservation across the shock front provides

$$c = \frac{v_{\mathrm{D}} - v_{\mathrm{i}}}{\varepsilon_{\mathrm{D}}}, \tag{2}$$

while momentum conservation of the incident end of the foam and the free mass gives

$$m v_0 = \left(M + m\frac{s}{L}\right) v_{\mathrm{i}} + m\left(1 - \frac{s}{L}\right) v_{\mathrm{D}}. \tag{3}$$

Eqs. (2) and (3), written in non-dimensional form, lead to

$$\frac{c}{v_0} = \frac{(1+\bar{m})\bar{v}_{\mathrm{D}} - \bar{m}}{\varepsilon_{\mathrm{D}}(\bar{m}\bar{s}+1)} \tag{4}$$

where $\bar{m} \equiv m/M$ is the mass ratio. Substitution of Eq. (4) into Eq. (1b) provides

$$(1-\bar{s})\frac{\mathrm{d}\bar{v}_{\mathrm{D}}}{\mathrm{d}\bar{s}} = -\frac{\sigma_{\mathrm{Y}}}{\rho v_0^2}\frac{\varepsilon_{\mathrm{D}}(\bar{m}\bar{s}+1)}{(1+\bar{m})\bar{v}_{\mathrm{D}} - \bar{m}} \tag{5}$$

and this may be integrated, with the initial conditions $\bar{v}_{\mathrm{D}} = 1$ at $\bar{s} = 0$, to give

$$\bar{v}_{\mathrm{D}}^2 - \frac{2\bar{m}}{1+\bar{m}}\bar{v}_{\mathrm{D}} - \frac{2\eta}{1+\bar{m}}[\ln(1-\bar{s}) + \bar{m}(\bar{s} + \ln(1-\bar{s}))] - \frac{1-\bar{m}}{1+\bar{m}} = 0, \tag{6}$$

where

$$\eta \equiv \frac{\sigma_{\mathrm{Y}}\varepsilon_{\mathrm{D}}}{\rho v_0^2}. \tag{7}$$

Note that η is a governing dimensionless group and is the ratio of static strength of the foam to the hydrodynamic pressure $\rho v_0^2/\varepsilon_{\mathrm{D}}$ within the foam; along with the mass ratio $\bar{m}$ it dictates the solution space. Relation (6) gives the non-dimensional velocity $\bar{v}_{\mathrm{D}} = v_{\mathrm{D}}/v_0$ as a function of location $\bar{s} = s/L$ of the shock front. In order to obtain the relation between $\bar{v}_{\mathrm{D}}$ and time t, it is necessary to relate t to $\bar{s}$. Upon recalling that $c(s) = \mathrm{d}s/\mathrm{d}t$, we have

$$t = \int_0^s \frac{\mathrm{d}s'}{c(s')} \tag{8}$$

and the non-dimensional time follows from Eq. (4) as

$$\bar{t}(\bar{s}) \equiv \frac{v_0 t}{L\varepsilon_{\mathrm{D}}} = \int_0^{\bar{s}} \left[\frac{(\bar{m}\bar{s}+1)}{(1+\bar{m})\bar{v}_{\mathrm{D}} - \bar{m}}\right] \mathrm{d}\bar{s}. \tag{9}$$

Thus, the relation between $\bar{v}_{\mathrm{D}}$ and $\bar{t}$ is known parametrically in terms of $\bar{s}$ by Eq. (6) and by the quadrature formula (9).

It remains to obtain expressions for the pressure p imposed by the foam on the free mass and for the arrest time τ of the shock wave. To proceed, we need to determine the stress σ_{i} on the downstream face of the shock wave. The usual expression for momentum conservation across the

shock wave gives

$$(\sigma_{\mathrm{i}} - \sigma_{\mathrm{Y}}) = -\rho c(v_i - v_{\mathrm{D}}) \tag{10}$$

and elimination of c via Eq. (2) leads to

$$\sigma_{\mathrm{i}} = \sigma_{\mathrm{Y}} + \frac{\rho(v_{\mathrm{D}} - v_i)^2}{\varepsilon_{\mathrm{D}}}. \tag{11}$$

Relation (11) displays the elevation in stress downstream of the shock wave due to material inertia. Upon eliminating v_{i} via Eq. (3) we obtain

$$\frac{\sigma_i}{\sigma_{\mathrm{Y}}} = 1 + \frac{1}{\eta}\left[\frac{(1+\bar{m})\bar{v}_{\mathrm{D}} - \bar{m}}{(\bar{m}\bar{s}+1)}\right]^2. \tag{12}$$

Thus, σ_{i} is known explicitly in terms of $\bar{s}$ by Eqs. (6) and (12). Further, a direct connection exists between the contact pressure p and σ_{i} according to

$$\dot{v}_{\mathrm{i}} = \frac{p}{M} = \frac{\sigma_i}{M + m\bar{s}} \tag{13}$$

and so the non-dimensional pressure $\bar{p} \equiv p\varepsilon_{\mathrm{D}}/(\rho v_o^2)$ is

$$\bar{p}(\bar{s}) = \frac{\eta}{\bar{m}\bar{s}+1}\left\{1 + \frac{1}{\eta}\left[\frac{(1+\bar{m})\bar{v}_{\mathrm{D}} - \bar{m}}{\bar{m}\bar{s}+1}\right]^2\right\}. \tag{14}$$

Relation (9) is used to write $\bar{s}$ in terms of $\bar{t}$.

The shock wave arrests when the two velocities v_{i} and v_{D} attain a common final value v_{f} as specified by the momentum relation

$$(M+m)v_{\mathrm{f}} = mv_0. \tag{15}$$

Thus, the non-dimensional final velocity $\bar{v}_{\mathrm{f}}$ is

$$\bar{v}_{\mathrm{f}} \equiv \frac{v_{\mathrm{f}}}{v_0} = \frac{\bar{m}}{1+\bar{m}}. \tag{16}$$

The arrest distance of the shock wave s_{f} follows from Eq. (6) by noting that $s = s_{\mathrm{f}}$ at $\bar{v}_{\mathrm{D}} = \bar{v}_{\mathrm{f}}$,

$$2\eta(1+\bar{m})^2\ln(1-\bar{s}_{\mathrm{f}}) + 2\eta\bar{m}(1+\bar{m})\bar{s}_{\mathrm{f}} + 1 = 0. \tag{17}$$

In the extreme dynamic limit $\eta \to 0$, Eq. (17) gives the asymptotic limit,

$$\bar{s}_{\mathrm{f}} \to 1 - \exp\left(-\frac{1}{2\eta(1+\bar{m})^2}\right), \tag{18a}$$

while in the quasi-static limit, $\eta \to \infty$ and

$$\ln(1-\bar{s}_{\mathrm{f}}) + \frac{\bar{m}}{1+\bar{m}}\bar{s}_{\mathrm{f}} \to 0 \tag{18b}$$

giving $\bar{s}_{\mathrm{f}} \to 0$. Thus, $\bar{s}_{\mathrm{f}}$ lies in the range $0 \leqslant \bar{s}_{\mathrm{f}} \leqslant 1$ in all cases: the plastic shock wave always arrests before it reaches the end of the foam projectile.

Similarly, the arrest time τ is specified in the non-dimensional form

$$\bar{\tau} \equiv \frac{v_0 \tau}{L \varepsilon_D} \tag{19}$$

by integrating Eq. (9) with an upper limit of integration of $\bar{s} = \bar{s}_f$. Note that the non-dimensional final velocity $\bar{v}_f$ depends only upon the mass ratio $\bar{m}$, while the non-dimensional arrest distance $\bar{s}_f$ and arrest time $\bar{\tau}$ are functions of both $\bar{m}$ and η.

The analysis presented above has some similarities to those of Reid and Peng [10] and Tan et al. [3] for the dynamic crushing of wood and Hydro aluminium foam, respectively. In these previous studies, a heavy backing disk was attached to the back face of the projectile and the impacted mass was considered to be motionless. The current analysis can be brought into alignment with these previous studies for the case of a massless backing disk and the choice $\bar{m} = 0$.

2.1. Predictions

The contact pressure $\bar{p}$ versus time $\bar{t}$ curve is plotted in Fig. 2a for selected values of the strength ratio η and mass ratio $\bar{m}$. First, consider the dynamic case $\eta = 0.05$, such that the dynamic pressure $\rho v_0^2/\varepsilon_D$ is twenty times the static collapse strength σ_Y of the foam. As $\bar{t} \to 0$, $\bar{p} \to 1 + \eta$ and thus $\bar{p}(\bar{t} = 0) = 1.05$ for all $\bar{m}$. For the choice $\bar{m} = 0$, the pressure versus time response is reasonably flat up to the shock arrest time $\bar{\tau}$. This feature results from the fact that the impacted end of the foam is stationary while the distal end moves at almost constant velocity equal to the initial velocity of the foam. With increasing $\bar{m}$, the pressure decreases with time for all $\bar{t} > 0$. Similarly in the almost quasi-static case, $\eta = 1$, the pressure drops sharply with increasing time for all $\bar{m}$. Note that the pressure has a finite value, without dropping to zero, at the shock arrest time $\bar{\tau}$. This is explained as follows. The model described above neglects elastic effects and gives no information on the pressure history beyond the shock arrest time, $\bar{t} = \bar{\tau}$. The inclusion of an elastic unloading branch to the constitutive description would lead to a continuous reduction in $\bar{p}$ to zero after the plastic shock wave has arrested.

The velocity v_i of the free mass, as normalised by the final velocity v_f, is plotted against time $\bar{t}$ in Fig. 2b for $\eta = 0.05$ and 1, and for a mass ratio $\bar{m}$ in the range 0.005 to 3. (The limit $\bar{m} = 0$ is a degenerative case as $v_i = v_f = 0$.) In the dynamic case, $\eta = 0.05$, the velocity versus time response is rather non-linear while v_i increases approximately linearly with $\bar{t}$ in the almost quasi-static case $\eta = 1$.

The shape of the pressure pulse can be described by the ratio of mean pressure p_m over the pulse duration,

$$p_m = \frac{1}{\tau} \int_0^{\tau} p(t)\, \mathrm{d}t \tag{20}$$

to the initial peak pressure p_{peak}. This ratio is plotted against η in Fig. 3 for selected values of $\bar{m}$. Consistent with the pressure histories plotted in Fig. 2a, p_m/p_{peak} decreases with increasing $\bar{m}$ at any given value of η. Moreover, the ratio p_m/p_{peak} displays a minimum at an intermediate value of η.

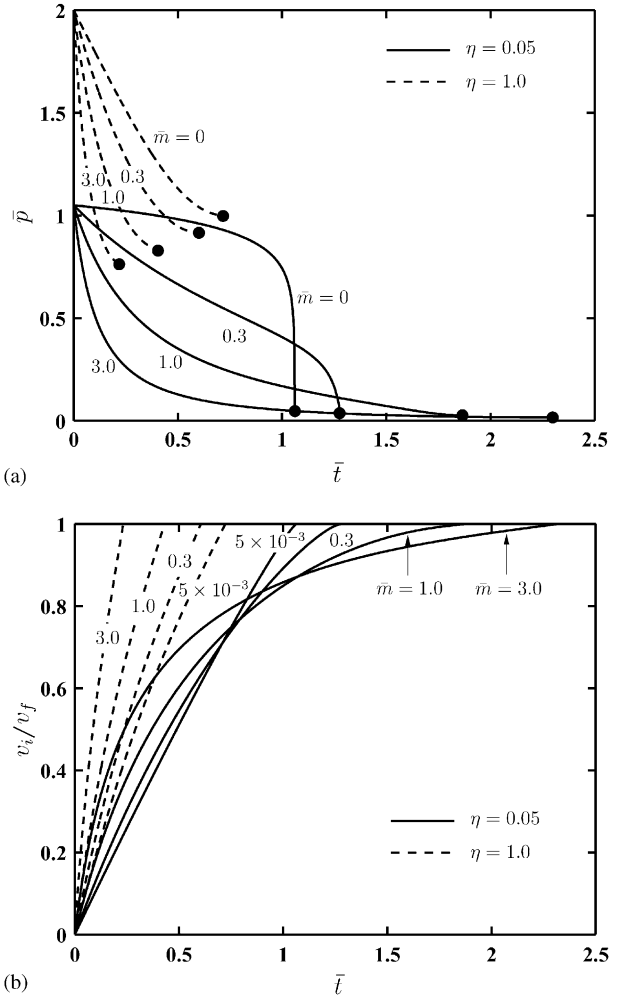

Fig. 2. Predicted time histories of the (a) normalised contact pressure and (b) impacted mass velocity for two choices of strength ratio η. The histories are shown for selected values of the mass ratio $\bar{m}$.

The normalised shock arrest time $\bar{\tau}$ and the normalised shock arrest distance $\bar{s}_f$ are plotted against η in Figs. 4a and b, respectively, for selected values of $\bar{m}$. Note that $\bar{\tau} = 1$ has the interpretation that the average plastic shock wave speed equals v_0/ε_D. In the dynamic limit $\eta \approx 0$, $\bar{\tau}$ increases with increasing $\bar{m}$ whereas in the quasi-static limit ($\eta \geqslant 1$) $\bar{\tau}$ decreases with increasing $\bar{m}$. At large values of $\bar{m}$, τ decreases sharply with increasing η; this leads to the increase in p_m/p_{peak} with increasing η seen in Fig. 3. Next, consider the shock arrest distance $\bar{s}_f$. For any assumed value of $\bar{m}$, $\bar{s}_f$ decreases from unity to zero as η increases from zero to infinity, as seen in Fig. 4b; this observation has already been made via an analytical argument above. We further note that $\bar{s}_f$ increases with decreasing $\bar{m}$, for any assumed value of η.

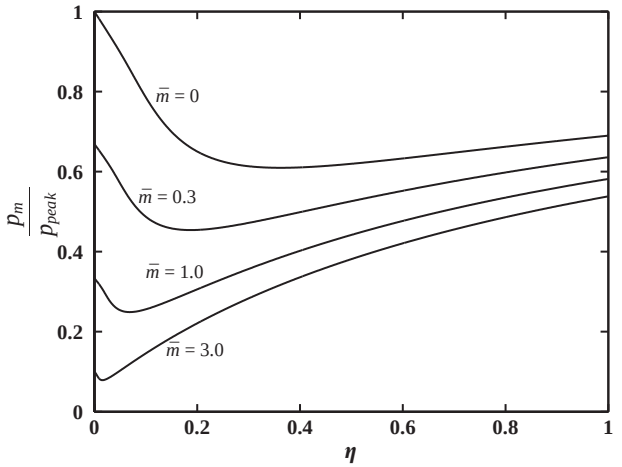

Fig. 3. The predicted ratio of the average contact pressure p_{m} to the peak contact pressure p_{peak} as a function of the strength ratio η for selected values of mass ratio $\bar{m}$.

2.2. Structure of the shock wave

In the above analysis no statement has been made of energy conservation within the shock wave, but only an equilibrium statement that momentum is conserved across the shock wave. Introduce γ as the quasi-static plastic work of the foam (equal to the area under the quasi-static stress versus strain curve) normalised by the total drop in kinetic energy of foam and target during the shock event. Then, via Eq. (3) we have

$$\gamma = 2\eta(1 + \bar{m})\bar{s}_{\mathrm{f}}. \tag{21}$$

This ratio lies in the range $0 < \gamma < 1$. Thus, it is assumed implicitly within the above analysis that a dissipative mechanism is operative in addition to the quasi-static plastic dissipation to account for the loss in energy at the moving shock front. This additional dissipation dominates the quasi-static plastic work at small values of η: it is evident from relations (18a) and (21) that $\gamma \to 0$ as $\eta \to 0$.

A detailed description of dissipation within the moving shock wave requires additional constitutive assumptions, and the simplest possible approach is to introduce linear rate dependence. In Appendix A we show that a linear rate dependence of strength of the foam leads to a shock of finite thickness, with a continuous velocity and stress distribution within the shock. The analysis is asymptotic in nature by assuming that the shock wave travels at a uniform velocity. With this modified constitutive description, it is shown explicitly that the total dissipation within the shock equals the drop in kinetic energy, as demanded by an energy audit. The internal structure of the shock wave is predicted, with the jump conditions across the shock wave still given by Eq. (11). Previous treatments of plastic shock wave propagation within metal foams, see Ashby et al. [1] and Tan et al. [3] implicitly assume that additional dissipative mechanisms exist within the shock wave, but do not explore the shock structure.

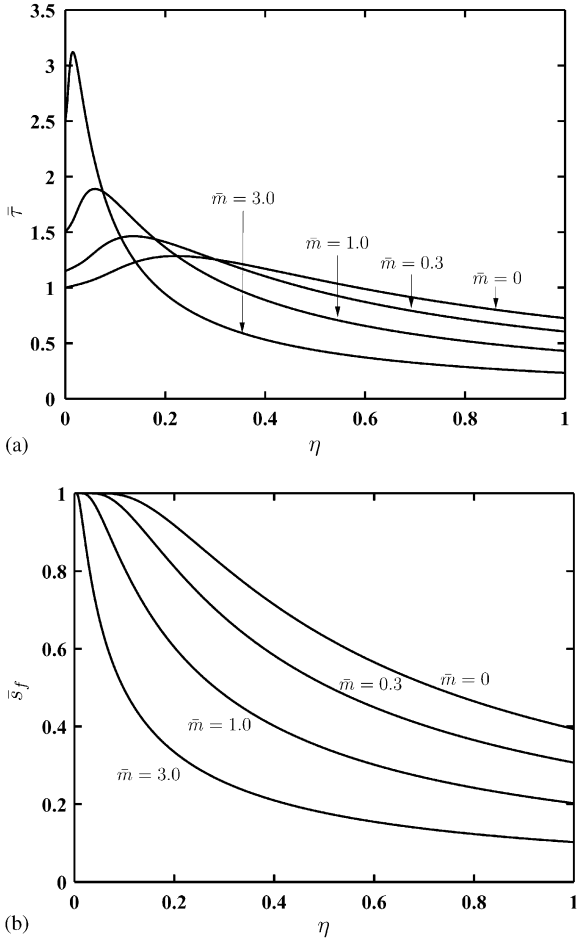

Fig. 4. Predictions of the (a) shock arrest time and (b) shock arrest distance as a function of the strength ratio η for selected values of the mass ratio $\bar{m}$.

3. Experimental program

3.1. Metal foam projectiles

Circular, cylindrical projectiles of length L in the range 50–100 mm and diameter 28.5 mm were electro-discharge machined from a block of closed cell aluminium foam Alporas,[1] of relative density $\bar{\rho}$ in the range of 11–17%. The Alporas foam is of composition Al-Ca 5-Ti 3 (wt.%), and of average cell size 4 mm.

The quasi-static compressive response of the foam of relative density 11% is given in Fig. 5, at a nominal strain rate of $10^{-3}\,s^{-1}$, for circular cylindrical specimens of length 50 mm and diameter 28.5 mm. In addition to uniaxial stressing (without lateral confinement) uniaxial straining tests

[1]Shinko Wire Co. Ltd., Amagasaki, Japan.

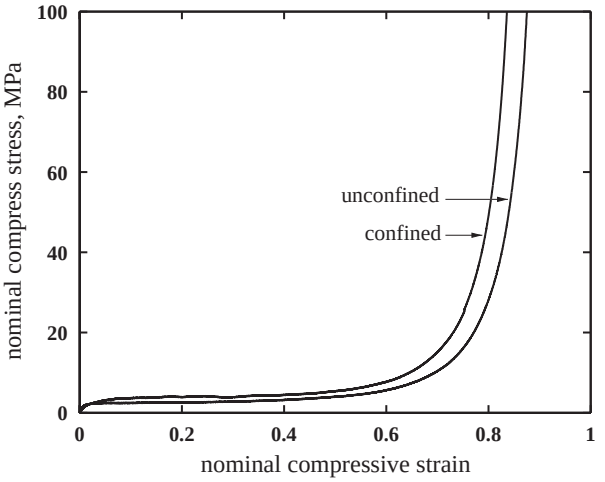

Fig. 5. Measured quasi-static compressive response of the $\bar{\rho} = 0.11$ Alporas foam with lateral expansion inhibited (confined) and free lateral expansion (unconfined).

were performed: full constraint against radial expansion was achieved by placing the specimens inside a lubricated circular steel die with a clearance fit. It is clear from Fig. 5 that lateral confinement has only a small effect upon the compressive response; this is consistent with the fact that the Alporas foam has a plastic Poisson ratio close to zero, as observed by Deshpande and Fleck [11]. The foam has a compressive plateau strength of 3.0 MPa in the confined state, and a nominal lock-up strain of approximately 0.8.

3.2. Direct impact tests

Direct impact experiments in which foam projectiles were fired at a strain gauged Kolsky bar [12,13] were performed and the pressure versus time history at the impacted end of the foam projectiles measured along with high-speed photographic observations of the plastic shock waves within the foam.

The set-up of the Kolsky pressure bar is standard and made use of a mild steel circular bar of length 1.8 m and diameter 28.5 mm. After impacting one end of the bar by the foam projectiles, the contact pressure history on the impacted end of the bar was measured via strain gauges placed approximately 10 diameters from the impact end of the bar. The elastic strain histories in the bars were monitored using two TML foil gauges of length 1 mm in a Wheatstone bridge configuration. A strain bridge amplifier of cut-off frequency 500 kHz was used to provide the bridge input voltage and a digital storage oscilloscope was used to record the output. The bridge system was calibrated dynamically over the range of strains measured during the experiments and was determined to be accurate to within 1%. The longitudinal elastic wave speed was measured to be $5155\,\mathrm{m\,s^{-1}}$, giving a time-window of 600 μs before elastic reflections from the distal end of the bar complicate the measurement of pressure. In a number of the experiments, high-speed photographic sequences were taken using a Hadland 790 camera, thereby allowing observation of the deformation process.

The metal foam projectiles were accelerated using a gas gun of barrel length 4.5 m and diameter 28.5 mm, as detailed in [14]. No sabot was employed, and the bursting of copper shim diaphragms formed the breech mechanism of the gun. The impact experiments were performed at velocities ranging from approximately 50 to 500 m s^{-1}. The velocity of the projectile was measured at the exit of the barrel using laser-velocity gates. The impacted end of the Kolsky bar was placed 100 mm from the end of the gun barrel. A series of experiments was performed in order to measure the effect of foam density, projectile length and velocity upon the pressure versus time response.

3.3. Normal impact of a free mass

A separate series of experiments was performed involving the impact of a freestanding metal disk by the foam projectile. The theoretical analysis of Section 2 suggests that the contact pressure versus time history imparted by the foam projectile upon the target is sensitive to the mass ratio $\bar{m}$ of foam to target disk. In these experiments, high-speed photography was used to measure the displacement of the target after impact. A measurement scale was placed in the line of sight of the camera, and images of the target were taken at known time intervals in order to measure the displacement.

The target disks were made from mild steel of thickness $h = 38$ mm and from 2014A-T3 aluminium alloy of $h = 10$ mm, and were machined to a diameter of 28.5 mm (identical to that of the foam projectiles). These disks rested upon two lubricated support guides with the normal to their faces along the gun barrel, and were located 50 mm from the end of the barrel. The foam projectiles employed had a relative density of 11% and length 100 mm. Experiments were performed with $\bar{m}$ held fixed at 0.1 (steel disk) and 1.1 (aluminium alloy disk), and at 3 impact velocities v_0 between 100 and 450 m s^{-1}.

4. Experimental results and comparison with theory

4.1. Direct impact tests

4.1.1. Observations

A high-speed photographic sequence of a direct impact experiment is shown in Fig. 6. The foam projectile was of length $L = 50$ mm, of relative density 11% and was fired at a velocity of 381 m s^{-1}. The exposure time of each photograph was 4 μs and the interframe times were 20 μs. The sequence of images reveals the propagation of a plastic shock wave from the impact face of the foam projectile. The distal portion of the projectile remains almost undeformed prior to arrival of the compression wave. The shock event occurs as a planar wave and direct observations after the impact event confirmed that the foam deformation occurred with negligible radial expansion. A cloud of dust is evident in the photographs, and was due to the brittle fragmentation of the foam cells at the shock front.

The high-speed photography suggests that the shock wave has a sharp front. To gain insight into the structure of the shock front, the specimen shown in Fig. 6 was sectioned along its diametrical plane after the test. The scanning electron micrograph shown in Fig. 7 confirms that

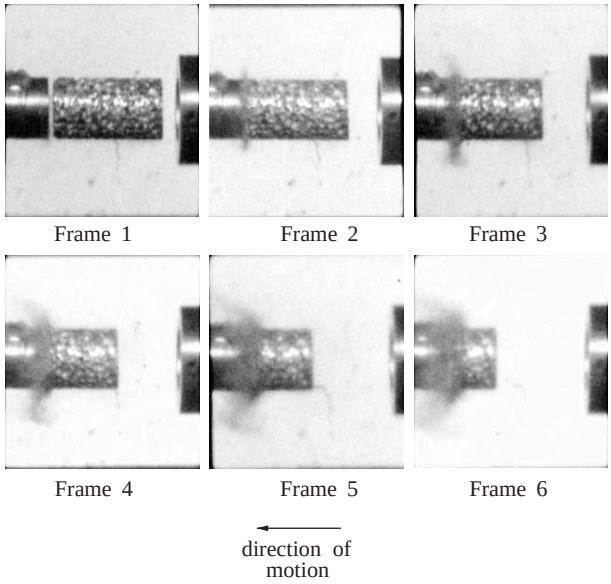

Fig. 6. A high-speed photographic sequence of the $\bar{\rho} = 0.11$ Alporas foam impacting a Kolsky pressure bar at $381\,\mathrm{m\,s^{-1}}$. The inter-frame time is $20\,\mu\mathrm{s}$.

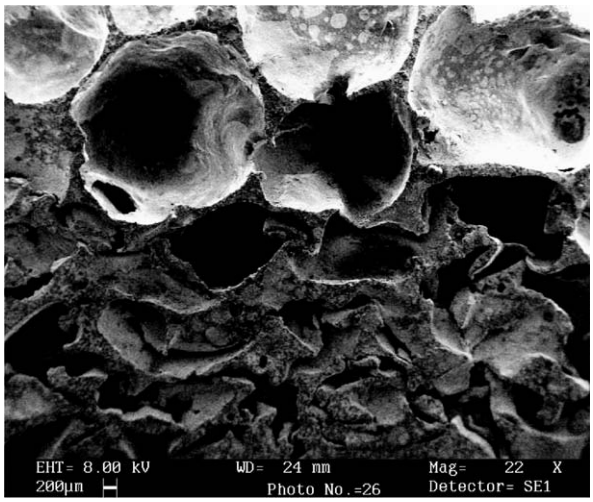

Fig. 7. A scanning electron micrograph of the metal foam specimen shown in Fig. 6 and sectioned along its diametrical plane. The micrograph clearly shows a sharp shock front separating the compressed and undeformed regions of the foam.

the shock front spanned a single cell (of dimension about 4 mm), with no observable plastic deformation at the distal end of the foam projectile. The impacted end is significantly compacted and comparisons with the deformed microstructure in quasi-static experiments suggest that the axial nominal strain in the compacted portion is of magnitude approximately 0.8.

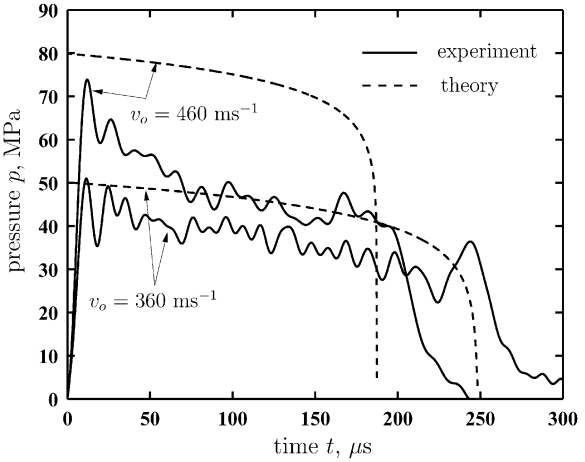

Fig. 8. The measured contact pressure histories of the $\bar{\rho} = 0.11$ Alporas foams of length $L = 100$ mm at two selected values of impact velocity in the direct impact Kolsky bar experiments. Theoretical predictions of the pressure histories are included.

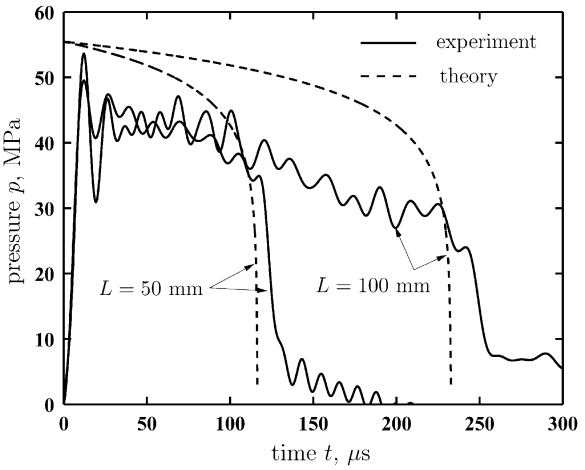

Fig. 9. The measured contact pressure histories of the $\bar{\rho} = 0.11$ Alporas foams of length $L = 50$ and 100 mm ($v_0 = 380\,\mathrm{m\,s^{-1}}$) in the direct impact Kolsky bar experiments. Theoretical predictions of the pressure histories are included.

4.1.2. Measured pressure history

The effect of impact velocity, projectile length and foam density upon the pressure versus time response is shown in Figs. 8–10, respectively. Unless otherwise stated, the reference test conditions are a projectile of length $L = 100$ mm and foam relative density of 11%.

First, it is seen from Fig. 8 that a 25% increase in impact velocity from 360 to 460 m s^{-1} leads to an increase in peak pressure of approximately 50%, and to an increase in average pressure of approximately 25%. The duration of the pulse decreases by about 20%. The predicted pressure histories have been added to Fig. 8, for the appropriate choice of parameters ($\sigma_Y = 3.0$ MPa and

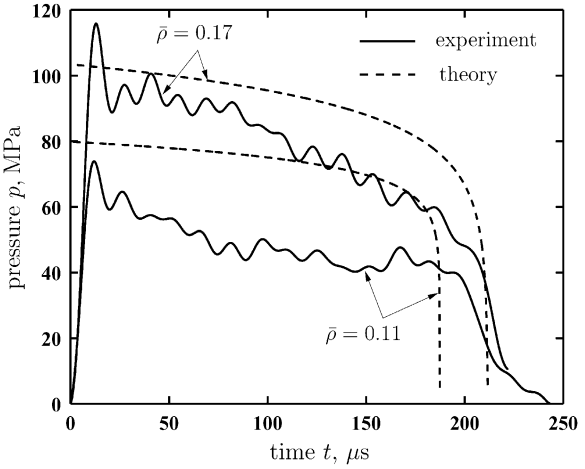

Fig. 10. The measured contact pressure histories of the $\bar{\rho} = 0.11$ and 0.17 Alporas foams of length $L = 100\,\text{mm}$ in the direct impact Kolsky bar experiments. The impact velocities of the 11% and 17% density foams were 460 and $420\,\text{m s}^{-1}$, respectively. Theoretical predictions of the pressure histories are included.

$\varepsilon_D = 0.82$, giving $\eta \approx 0.065$ for $v_0 = 360\,\text{m s}^{-1}$, and $\eta \approx 0.04$ for v_0 $460\,\text{m s}^{-1}$, with $\bar{m} = 0$ in both cases). The theory successfully captures the peak stress and the pulse duration, but over predicts the average pressure by about 20–40%. The shape of the predicted response adequately mimics the measured behaviour. It is believed that the rapid oscillations in measured pressure are due to the fact that the crush bands are not uniform across the width of the specimen.

Second, the pressure versus time response for $L = 50$ and $100\,\text{mm}$ is given in Fig. 9, for a relative density of 11% and for an impact velocity $v_0 = 360\,\text{m s}^{-1}$. The predictions are included in the figure and are in reasonable agreement with the measurements. The predicted pressure versus time trace is stretched by a factor of 2 when the length L is doubled; this feature is borne out by the experiments.

Third, upon increasing the relative density from 11% to 17% the pressure increases by about 50%, for specimens of length $L = 100\,\text{mm}$, as seen in Fig. 10. The measured velocity was $460\,\text{m s}^{-1}$ for the foam of relative density 11% and $420\,\text{m s}^{-1}$ for the foam of relative density 17%. Again, the predictions of the peak pressure and pulse duration are in good agreement with the experimental data while the theory over predicts the average pressure by 20–40%.

In Figs. 8–10, the experimental measurements indicate the initial peak stress is not captured by the theoretical predictions. This discrepancy between model and the experiments may be due to several reasons including the following two:

(i) The continuum model ignores dynamic strengthening mechanisms such as micro-inertia stabilisation of the buckling of the foam cell walls.
(ii) The foam is modelled as a rate independent solid: a visco-plastic model for the foam will predict that upon impact, the foam attains a peak stress $p_{\text{peak}} \approx \rho c_E v_0$, where c_E is the elastic wave speed of the foam, before a plateau in the stress is attained.

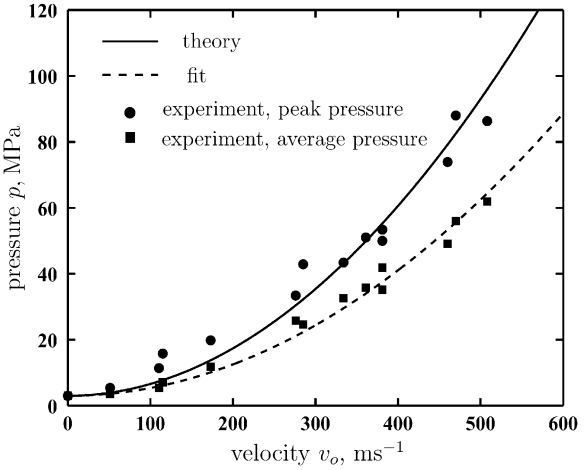

Fig. 11. The measured peak and mean contact pressures of the $\bar{\rho} = 0.11$ Alporas metal foams as a function of the impact velocity v_0 in the direct impact Kolsky bar experiments. The theoretical predictions for the peak pressure and a best fit-curve for the mean pressure are included.

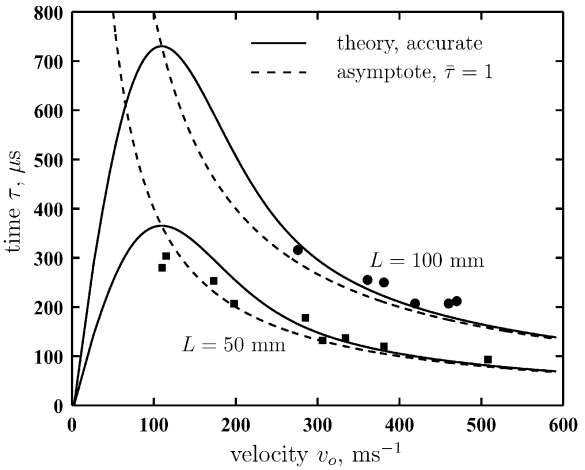

Fig. 12. The measured pulse duration of the $\bar{\rho} = 0.11$ Alporas metal foams as a function of the impact velocity v_0 in the direct Kolsky bar impact tests. Results are shown for two selected values of the foam length L. The theoretical predictions along with the asymptotes to the theory at large v_0 are included.

4.1.3. Summary of response

An extensive series of experiments were performed using foam projectiles of relative density 11% in order to determine the functional relationship between pressure history and impact velocity. The results for the peak pressure p_{peak} and mean pressure p_m, and the pulse duration τ are plotted against velocity v_0 in Figs. 11 and 12. The pulse duration is measured from the time when the pressure has attained 1/2 of the initial peak value to the time when the pressure has dropped half way down the trailing edge of the pressure history. Theoretical predictions for p_{peak}

and τ are included in the figures. The theoretical prediction of peak pressure is simply,

$$p_{\text{peak}} = \sigma_{\text{Y}} + \frac{\rho v_0^2}{\varepsilon_{\text{D}}}, \tag{22}$$

which agrees well with the experimental measurements. The theoretical predictions for the mean pressure are approximately equal to the peak pressure predictions and this theoretical line is not included in Fig. 11. The experimental data for the mean pressure is more accurately represented by the empirical fit,

$$p_{\text{m}} = \sigma_{\text{Y}} + 0.66\frac{\rho v_0^2}{\varepsilon_{\text{D}}} \tag{23}$$

as shown by the dashed line in Fig. 11. Again, this discrepancy between the experimental and theoretical predictions is most likely related to the fact that both the exact structure of the shock and rate sensitivity of the foam material have been neglected in the present model.

The asymptote for τ at large v_0 is included in Fig. 12 as a dashed line, and is given by $\bar{\tau} = 1$, with the simple interpretation that the plastic wave speed is constant at $v_0/\varepsilon_{\text{D}}$. This asymptote provides an adequate approximation to the measured response over the full range of projectile velocities and lengths considered in the current experimental study.

4.2. Normal impact of a free mass

The displacement versus time responses of the steel and aluminium disks after transverse impact by foam projectiles are plotted in Fig. 13a for $\bar{m} = 0.1$ and in Fig. 13b for $\bar{m} = 1.1$. The plots include the theoretical predictions (solid lines) by integration of Eq. (13) and the simpler prediction assuming a constant pressure on the disks equal to the initial peak value as given by Eq. (22). Note the predictions are shown to the point when the shock arrests in the foam; linear extrapolation will give the subsequent, constant velocity, response. Note that results are not included in Fig. 13b for the high velocity case $v_0 = 450\,\text{m}\,\text{s}^{-1}$ as preliminary experiments revealed that the target mass displaced by approximately 10 mm *before* impact, due to acceleration by the compressed air ahead of the projectile.

It is clear from Fig. 13 that the approximate theoretical prediction is adequate for small $\bar{m} = 0.1$. This result is consistent with the fact that the contact pressure remains almost constant during the impact event. In contrast, the pressure drops substantially with time for the case of a large $\bar{m} = 1.1$, as shown in Fig. 2a. Then, the full theory gives a more accurate prediction of the displacement versus time response over the range of impact velocities considered.

5. Concluding remarks

The use of metal foam projectiles to simulate water and air shock loading upon a structure has been developed. The technique is simple and safe to use in a laboratory setting and produces pressure histories representative of those observed in fluid shock loading.

The study has highlighted the existence of plastic shock waves in metal foams, and reveals that the energy dissipated within a shock front significantly exceeds the quasi-static energy absorption

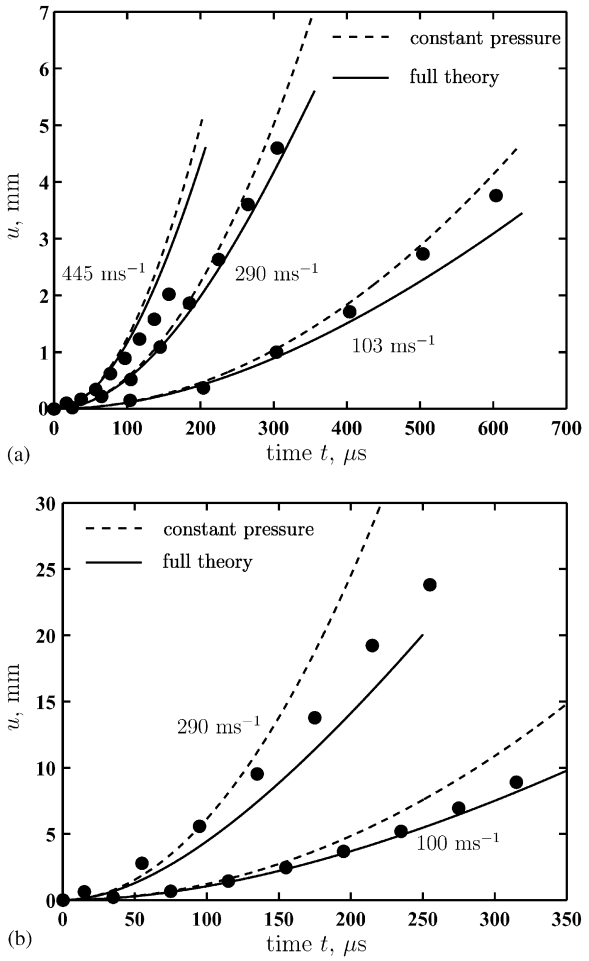

Fig. 13. Measured displacement versus time response of a free mass impacted by the $\bar{\rho} = 0.11$ Alporas foam for mass ratios (a) $\bar{m} = 0.1$ and (b) $\bar{m} = 1.1$ at selected impact velocities. Accurate theoretical predictions, and predictions assuming a constant contact pressure equal to the peak pressure, are included.

within the foam. A simple rate dependent constitutive law reveals a possible internal structure of the shock that accounts for the additional energy loss. The shock wave is predicted to have a thickness comparable to the cell size, and this is confirmed by experimental observation.

The pressure history imposed by the foam on the structure is sensitive to the areal mass ratio of foam projectile to structure. This mass ratio must be taken into account when using the foam projectile to replicate shock loadings. The theoretical predictions are supported by the experimental investigation, both for the pressure history on the end of a heavy structure (Kolsky pressure bar) and for the acceleration of a free standing mass. These results justify the use of the foam projectile as a means of dynamically loading practical structures such as sandwich beams, see for example Radford et al. [15].

Acknowledgements

The authors are grateful to ONR for their financial support through US-ONR IFO grant number N00014-03-1-0283 on The Science and Design of Blast Resistant Sandwich Structures and to the Isaac Newton Trust, Trinity College Cambridge.

Appendix A. An asymptotic analysis of the shock structure for a linear viscous foam

Consider a metal foam with a velocity jump Δv_0 across a planar shock front moving along the positive x direction at a constant velocity c. Equilibrium at time t of a material point of velocity v within the shock can be expressed as

$$\frac{\partial \sigma}{\partial \xi} = \rho \frac{\partial v}{\partial t} = -\rho c \frac{\partial v}{\partial \xi}, \tag{A.1}$$

where σ is the nominal compressive stress in the x direction, ρ is the initial density of the foam, and the convected co-ordinate ξ of the material point in a reference frame moving with the shock is $\xi = x - ct$.

Experimental observations from the direct impact Kolsky bar tests reveal that the shock front spans no more than one cell of the foam, see Fig. 6. Thus, for an impact velocity $v_0 = 400\,\mathrm{m\,s^{-1}}$, the strain-rate within the shock is approximately $400/4 \times 10^{-3} = 10^5\,\mathrm{s^{-1}}$. At these high strain rates, phonon drag governs plastic flow in metals, with the rate dependence well characterised by a linear viscous relation, see for example [16]. Thus, we employ a linear viscous constitutive relationship for the foam response

$$\sigma = \mu \dot{\varepsilon}, \tag{A.2}$$

where σ and $\dot{\varepsilon}$ are the nominal stress and nominal strain-rate, respectively and μ, the viscosity of the foam. Further, we specify that the foam undergoes no further deformation beyond a nominal densification strain ε_D. Combining Eqs. (A.1) and (A.2) gives the governing differential equation as

$$\frac{\partial^2 v}{\partial \xi^2} = -\frac{\rho c}{\mu} \frac{\partial v}{\partial \xi} \tag{A.3}$$

with solution

$$\frac{\partial v}{\partial \xi} = \dot{\varepsilon}(\xi) = \dot{\varepsilon}_0 \exp\left(-\frac{\xi}{l}\right), \tag{A.4}$$

where $\dot{\varepsilon}_0 \equiv \dot{\varepsilon}(\xi = 0)$ and $l = \mu/\rho c$. The velocity jump across the shock spanning $\xi = 0$ to ∞ is determined by integrating Eq. (A.4) and gives

$$\Delta v_0 = \dot{\varepsilon}_0 l. \tag{A.5}$$

Thus, the strain-rate at any material point ξ within the shock is given by

$$\dot{\varepsilon}(\xi) = \frac{\Delta v_0}{l} \exp\left(-\frac{\xi}{l}\right). \tag{A.6}$$

It remains to determine the shock propagation speed c. Recall that the foam undergoes no deformation beyond a nominal strain ε_D and hence material points exit the shock with this exit condition. Thus,

$$\varepsilon_D = -\frac{1}{c}\int_{\infty}^{0} \dot{\varepsilon}(\xi)\,d\xi, \tag{A.7}$$

which implies that the shock speed is

$$c = \frac{\Delta v_0}{\varepsilon_D}. \tag{A.8}$$

The shock width l can then be re-written as

$$l = \frac{\mu\varepsilon_D}{\rho\Delta v_0} \tag{A.9}$$

and the stress jump $\Delta\sigma$ across the shock is given by

$$\Delta\sigma = \mu\dot{\varepsilon}(\xi = 0) - \mu\dot{\varepsilon}(\xi = \infty) = \frac{\rho\Delta v_0^2}{\varepsilon_D} \tag{A.10}$$

consistent with the stress jump across the shock front employed in the analysis of Section 2. With the choice $\mu = 0.0006\,\text{MPa s}$ from [16], $\varepsilon_D = 0.83$, $\rho = 300\,\text{kgm}^{-3}$ and $\Delta v_0 = 300\,\text{ms}^{-1}$, the shock width is $l \approx 5.5\,\text{mm}$. This width is on the order of the cell size and is consistent with experimental observations, as seen in Fig. 6.

The above asymptotic analysis gives a continuous spatial distribution of stress and velocity and allows for a full energy audit: the rate of the viscous dissipation in the shock equals the drop in kinetic energy across the shock.

References

[1] Ashby MF, Evans AG, Fleck NA, Gibson LJ, Hutchinson JW, Wadley HNG. Metal Foams: A Design Guide, Vol. 1. Oxford: Butterworth-Heinemann; 2000.
[2] Fleck NA, Deshpande VS. The resistance of clamped sandwich beams to shock loading. J Appl Mech ASME 2004;71:386–401.
[3] Tan PJ, Harrigan JJ, Reid SR. Inertia effects in the uniaxial dynamic compression of a closed-cell aluminium alloy foam. J Mater Sci Technol 2002;18:480–8.
[4] Reddy TY, Reid SR, Barr RA. Experimental investigation of inertia effects in one-dimensional metal ring systems subjected to end impact—II free ended systems. Int J Impact Eng 1991;11:463–80.
[5] Reid SR, Bell WW, Barr RA. Structural plastic shock model for one-dimensional ring system. Int J Impact Eng 1983;1:175–91.
[6] Reid SR, Reddy TY, Peng C. Dynamic compression of cellular structures and materials. In: Jones N, Wierzbicki T editors. Structural Crashworthiness and Failure. Amsterdam: Elsevier Applied Science Publishers; 1993. p. 295.
[7] Zaretsky E, Ben-Dor G. Compressive stress-strain relations and shock Hugoniot curves of flexible foams. J Eng Mater Technol (Trans. ASME) 1995;117:278.
[8] Lopatnikov SL, Gama BA, Haque JM, Krauthauser C, Gilespie Jr JW, Guden M, Hall IW. Dynamics of metal foam deformation during Taylor cylinder–Hopkinson bar impact experiment. Composite Struct 2003;61:61–71.
[9] Lopatnikov SL, Gama BA, Haque JM, Krauthauser C, Gillespie Jr JW. High-velocity plate impact of metal foams. Int J Impact Eng 2004;30:421–45.

[10] Reid SR, Peng C. Dynamic uniaxial crushing of wood. Int J Impact Eng 1997;19:531–70.
[11] Deshpande VS, Fleck NA. Isotropic constitutive models for metallic foams. J Mech Phys Solids 2000;8:1253–83.
[12] Dharan CKH, Hauser FE. Testing techniques based on the split Hopkinson bar. Exp. Mech. 1970;10:370–6.
[13] Morgan JA, Carden AE. Dynamic compression of metal disks in the freight train experiment. In: Meyers MA editor. Metallurgical applications of shock-wave and high-strain-rate phenomena. New York: Marcel Dekker; 1986. p. 553–66.
[14] Radford DD. An experimental technique to study the response of structures to shock loading. Exp Mech 2004, submitted for publication.
[15] Radford DD, Deshpande VS, Fleck NA. The response of clamped sandwich beams subjected to shock loading. Int J Impact Eng, in press.
[16] Frost HJ, Ashby MF. Deformation-mechanism maps: The plasticity and creep of metals and ceramic. London: Pergamon Press; 1992.